This document is the unedited Author's version of a Submitted Work that was subsequently accepted for publication in Inorganic Chemistry, copyright © American Chemical Society after peer review. To access the final edited and published work see http://pubs.acs.org/articlesonrequest/AOR-sAKsiTihpAF4Ev2IFnNW.

Theoretical Study of Divalent

Bis(Pentaisopropylcyclopentadienyl) Actinocenes

Jason M. Yu and Filipp Furche*

Department of Chemistry, University of California Irvine, 1102 Natural Sciences II, Irvine,

CA 92697-2025, USA

E-mail: filipp.furche@uci.edu

Abstract

The existence of divalent bis(pentaisopropylcyclopentadienyl) actinocene compounds, $An(Cp^{iPr_5})_2$ for An = (Th, U, Pu, Am, Bk, No, Lr), is assessed by density functional theory (DFT) calculations with scalar-relativistic small core pseudopotentials. The calculations predict ground states with significant 6d occupation for Th, U, and Lr, whereas Am, Bk, and No exhibit 5f ground states. A mixed ground state with predominant 5f character is found for Pu. The complexes exhibit a linear coordination geometry and high S_{10} symmetry except for $Pu(Cp^{iPr_5})_2$ and $Am(Cp^{iPr_5})_2$, which are found to be bent by 11° and 12°, respectively. Absorption spectra are simulated with time-dependent density functional theory (TD-DFT) and compared to experimental spectra of known $tris(C_4H_4SiMe_3)$ and $tris(C_5H_3(SiMe_3)_2)$ compounds [M. E. Fieser et al., J. Am. Chem. Soc. 2015, 137, 369-382] as well as recently synthesized divalent lanthanide analogs Dy(Cp^{iPr₅})₂ and Tb(Cp^{iPr₅})₂ [C. Gould et al., J. Am. Chem. Soc. 2019, 141, 12967-12973. Thermodynamic stability is assessed by calculation of adiabatic reduction potentials of the trivalent precursors [An(CpiPr₅)₂]⁺, and the feasibility of further reduction to obtain as yet unknown monovalent molecular actinide complexes is discussed.

Introduction

Bis(cyclopentadienyl) metallocenes of the transition-metal elements are prototypical organometallic compounds. 1-4 The interaction of metal-centered valence d orbitals with ligand π orbitals in these species gives rise to rich coordination chemistry, enabling applications in numerous synthetic and catalytic purposes including stereoselective addition,⁵ olefin polymerization, ⁶⁻⁸ and N₂ activation. ⁹ A central goal of organoactinide chemistry is the discovery, isolation, and characterization of new compounds which exhibit chemistry similar to the transition-metals. However, π -bonded coordination compounds in low valence states are rare for the actinide elements, and no bis (cyclopentadienyl) actinocene analog exists. 10 From an electronic structure perspective, this discrepancy may be rationalized by the properties of the actinides' 5f valence shell, which is less favorable for coordinative bonding due to its contracted nature and high nodality. 11 Rather than forming bis(cyclopentadienyl) metallocenes known from transition metal elements, it was predicted by early calculations 12 and experimentally verified 13 that the actinides instead preferred tetravalent bis(COT) (COT = $\eta^8 - C_8 H_8$) structures with primarily electrostatic bonding. ^{14–17} Synthetic attempts towards bis(cyclopentadienyl) structures have produced linear or nearly linear species that include equatorial donor ligands bound to the metal. 18-20 Nevertheless, the higher metal oxidation states of these compounds preclude much of the organometallic activity exhibited by their transition-metal congeners.

Substituted cyclopentadienyl ligands $^{21-25}$ have led to the isolation of divalent lanthanide compounds containing three equatorial Cp" (Cp" = (C₅H₃(SiMe)₂)⁻¹)²⁶ and Cp' (Cp' = (C₅H₄SiMe₃)⁻¹) ligands. $^{27-29}$ Isolation of the actinide compounds [Th^{II}(Cp")₃]⁻¹, [U^{II}(Cp')₃]⁻¹, and [Pu^{II}(Cp")₃]⁻¹ followed soon after, with those for Th and U analogously exhibiting $(5f)^0(6d)^2$ and $(5f)^3(6d)^1$ configurations akin to transition-metal species. $^{30-33}$ A $(5f)^5(6d)^1/(5f)^6$ electron configuration was observed for [Pu^{II}(Cp")₃]⁻¹, whose HOMO has both d_{z^2} and f_{z^3} character. The unexpected discovery of divalent actinide compounds with substituted cyclopentadienyl groups suggested that other organoactinide compounds with unconventional

electronic structure could be accessed with suitable ligands.

Recently, divalent Dy and Tb complexes with bis(Cp^{iPr₅}) ligands (iPr = -CH(CH₃)₂) were synthesized by reduction of trivalent Ln(Cp^{iPr₅})₂I intermediates and characterized by X-ray crystallography, magnetic measurements, and density functional theory (DFT) calculations. Although bis(cyclopentadienyl) lanthanide species have been known since 1984,³⁴ these compounds represent the first linear or nearly-linear examples of lanthanide metallocenes.³⁵ These structures maintain a $(4f)^n(5d)^1$ ground state configuration and exhibit covalent σ -bonding between the cyclopentadienyl ligands and metal-based orbitals, resembling the bonding in transition-metal metallocenes.

Here we assess the viability of bis(pentaisopropylcyclopentadienyl) actinocene compounds (Figure 1) by characterizing the electronic structure of $An(Cp^{iPr_5})_2$ for An = (Th, U, Pu, Am, Bk, No, Lr). These species were chosen to illustrate variations in electronic structure between the early, intermediate, and late actinide elements due to the crossover of the 5f and 6d orbitals with increasing nuclear charge. Our computational methodology has been extensively validated in prior work on crystallographically characterized lanthanide complexes such as $Dy/Tb(Cp^{iPr_5})_2$, 35 [Ln{N(SiMe_3)_2}_3]⁻¹, 36 [Ln(C₅Me₄H)₃]⁻¹, 28 [Ln(Cp')₃]⁻¹, 1 [Ln(Cp")₃]⁻¹, 27,29 as well as the organoactinide complexes [Th(Cp")₃]⁻¹, 32 [U(Cp')₃]⁻¹, 30 [Pu(Cp")₃]⁻¹, 31 and U(C₅Me₄H)₃NO. 37 The current study focuses on key qualitative features of bis(Cp^{iPr₅}) actinide compounds including trends in dominant electronic configurations of the metal, symmetries, and properties relevant to guide synthetic efforts. More detailed calculations including spin-orbit interactions, a quantitative treatment of near-degeneracy effects, and a more complete description of low-lying excited states with different spin multiplicities are left to future work.

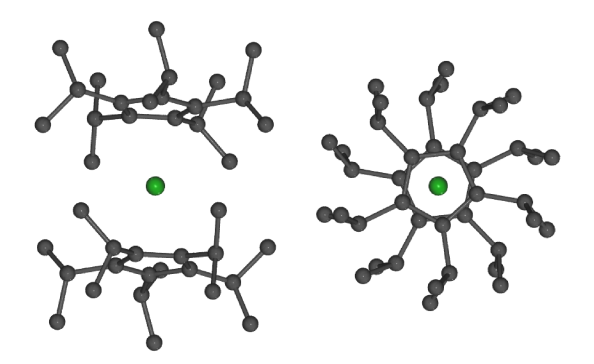


Figure 1: Side-on and end-on views of $An(Cp^{iPr_5})_2$ molecular structure. Hydrogen atoms are omitted for clarity.

Computational Details

Structure optimizations in the spin unrestricted formalism using the TPSS meta-generalized gradient approximation (meta-GGA)³⁸ density functional were performed for An(Cp^{iPr₅})₂ starting from the X-ray structure of Dy(Cp^{iPr₅})₂.³⁵ The An = (Th, No) compounds were found to possess closed shell valence configurations, and subsequent calculations on these species were performed with restricted spin orbitals. Stuttgart-Cologne scalar-relativistic small core effective core potentials (ECPs) were used for An = (Th, U, Pu, Am, Bk, No, Lr).³⁹ The corresponding valence basis set ^{40,41} was used for the actinide atoms, and a double- ζ quality basis set (def2-SV(P))⁴² was used for the ligands. The exchange-correlation terms were evaluated on a DFT quadrature grid of size m4 and total energies were converged in the SCF procedure to a tolerance of 10^{-7} hartrees. The resolution of the identity approximation (RI-J)⁴³ and D3 dispersion corrections by Grimme and co-workers⁴⁴ were employed.

Optimized structures were obtained to a maximum Cartesian gradient norm of 10^{-4} a.u. Each converged structure was verified to be a minimum by harmonic vibrational analysis.⁴⁵ Electronic configurations were assigned based on inspection of molecular orbitals and their natural atomic orbital populations.⁴⁶ Molecular coordinate files, orbital occupations, and visualizations of frontier orbital contours are available as supporting information (SI).

TD-DFT calculations to study electronic excitations were performed at optimized ge-

ometries with the gauge-invariant TPSSh hybrid functional. 38,47 Absorption spectra were simulated from the results using normalized Gaussian functions scaled by predicted oscillator strength. A root mean square width of 0.15 and empirical blue shift of 0.15 eV were used, consistent with parameters chosen to fit experimental spectra for the divalent lanthanocenes Dy/Tb(Cp^{iPr5})₂. 35 The lowest 10 dipole-allowed electronic excitations were computed for the S₁₀-symmetric structures An = (Th, U, Bk, No, Lr), and the lowest 30 dipole-allowed excitations were computed for the C₁-symmetric structures An = (Pu, Am). These numbers of roots approximately cover a spectral range of 250-1000 nm. To study the synthetic accessibility of the divalent and monovalent bis(Cp^{iPr5}) actinide compounds, implicit solvent corrections were included in DFT through the Conductor-like Screening Model (COSMO). These calculations were performed using the dielectric constant for tetrahydrofuran ($\epsilon = 7.520$). The harmonic oscillator-rigid rotor approximation at 298.15 K was used for free-energy calculations.

Molecular orbital plots were generated using the Visual Molecular Dynamics (VMD) program with a contour value of 0.03.⁵⁰ All electronic structure calculations were performed with the TURBOMOLE 7.3 quantum chemistry software package.⁵¹

Results

Electronic Structure

Dominant An electron configurations, ground state term symbols, frontier orbital energies, and metal-centroid distances are displayed in Table 1 and Figure 2. In all $An(Cp^{iPr_5})_2$ species, the An 6d orbitals split into orbitals transforming according to the a_g , e_{1g} and e_{2g} irreducible representations of the S_{10} point group, ordered by increasing energy in the ligand field. The 5f shell is split into two sets of degenerate orbitals transforming as e_{2u} , one set of degenerate orbitals as e_{1u} , and one orbital as a_u . The relative energies of the An 5f orbitals differ by actinide: Th, Am, No, and Lr possess an α spin orbital ordering of $(e_{2u}, e_{2u}, a_u, e_{1u})$

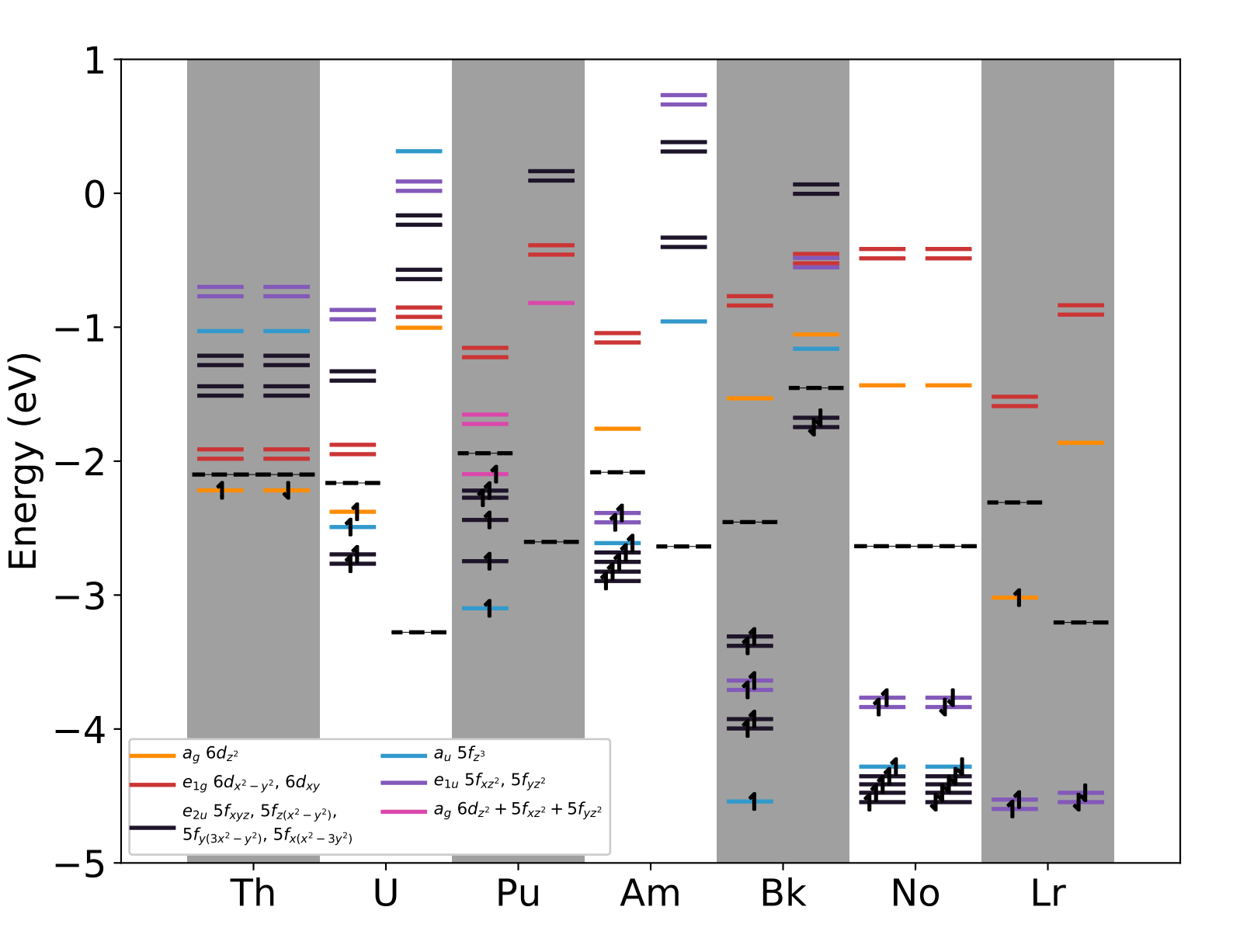


Figure 2: Frontier molecular orbital diagram in the spin unrestricted formalism for α (left) and β (right) spins labeled by term symbol and function for $Ac(Cp^{iPr_5})_2$ An = (Th, U, Pu, Am, Bk, No, Lr). Orbital energies were computed with DFT using the TPSS functional and small core ECPs for each An atom. Fermi levels are denoted with a dashed line. Visualizations of each orbital contour are provided as SI. The 6d orbitals transforming as e_{2g} occur above 1 eV and are not included for simplicity.

Table 1: Assigned electronic configurations, term symbols, HOMO and LUMO energies (eV), HOMO-LUMO energy gaps (eV), metal-centroid bond lengths (Å), and bond length differences with known tris(Cp'/Cp'') structures for $An(Cp^{iPr_5})_2$, (An = Th, U, Pu, Am, Bk, No, Lr).

	Config.	Term	$E_{\rm HOMO}({ m eV})$	$E_{\rm LUMO}(eV)$	$\Delta E_{\rm gap}(eV)$	M - $Cp(\mathring{A})$	$\Delta[(Cp)_3 - (Cp^{iPr_5})_2](\mathring{A})$
Th	$(6d)^2$	$^{1}A_{g}$	-2.218	-1.982	0.236	2.534	0.004
U	$(5f)^3(6d)^1$	5A_g	-2.378	-1.948	0.430	2.483	0.038
Pu	$(5f)^{6\dagger}$	7A	-2.097	-1.785	0.289	2.490*	0.032
Am	$(5f)^{7}$	8A	-2.408	-1.758	0.233	2.542*	
Bk	$(5f)^9$	6A_g	-1.746	-1.531	0.215	2.455	
No	$(5f)^{14}$	$^{1}A_{g}^{-}$	-3.836	-1.434	2.402	2.442	
Lr	$(5f)^{14}(6d)^1$	$^{2}A_{g}$	-3.019	-1.863	1.156	2.417	

[†] Pu possesses a mixed configuration with $(5f)^6$ and $(5f)^5(6d)^1$ character

in increasing order, whereas U and Pu possess orderings that place the a_u orbital between or before the two sets of e_{2u} orbitals, respectively. For Bk, the placement of orbitals with both a_u and e_{1u} symmetry results in an α spin orbital ordering of $(a_u, e_{2u}, e_{1u}, e_{2u})$.

Ground state configurations of $(5f)^0(6d)^2$ and $(5f)^3(6d)^1$ were found for Th(Cp^{iPr₅})₂ and U(Cp^{iPr₅})₂, respectively, giving rise to a highest occupied molecular orbital (HOMO) with both $6d_{z^2}$ and 7s character. Symmetry-allowed $6d_{z^2} - 7s$ mixing increases the stabilization of this orbital relative to the 5f shell. The orbital contour for U(Cp^{iPr₅})₂ is visualized in Figure 3. Qualitatively similar HOMOs are also found in the Ln(II) metallocenes Dy(Cp^{iPr₅})₂ and Tb(Cp^{iPr₅})₂, suggesting that the linear coordination environment facilitates such orbital mixing. Indeed, the corresponding tris(Cp') and tris(Cp'') structures for both Ln(II) and An(II) species contain a HOMO lacking significant s character.

The HOMO of $Pu(Cp^{iPr_5})_2$ has mixed 5f and $6d_{z^2}/7s$ character, indicating that the Pu compound corresponds to a configurational crossover between the $(5f)^n(6d)^1$ configurations of the early Th and U compounds and the $(5f)^{n+1}$ configurations of the later Am and Bk compounds in the series. Natural atomic populations arising from the actinide atom for the HOMO are presented in Table 2, along with those for the U and Bk compounds to illustrate the orbital mixing. The configurational crossover near Pu is also observed in both the tris(Cp') and tris(Cp') environments, 31 demonstrating its tendency to exhibit

^{*} Averaged between the two M-Cp^{iPr₅} distances

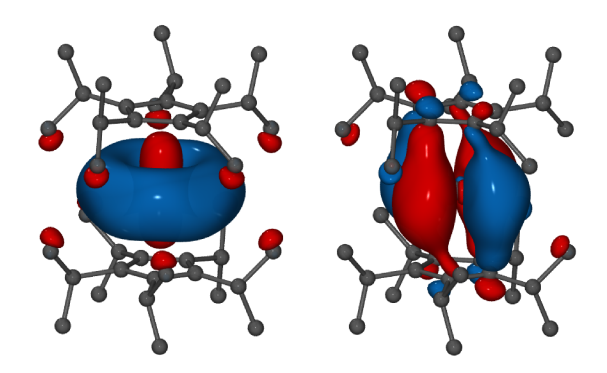


Figure 3: Contour plot of HOMO and LUMO for $U(Cp^{iPr_5})_2$ at 0.03 isovalue computed with DFT using the TPSS functional.

nearly-degenerate 6d and 5f shells in structures with cyclopentadienyl ligands. A precise characterization of the ground state for these systems may require multireference wavefunction approaches beyond DFT. The HOMO and LUMO contours for the Pu structure are visualized in Figure 4.

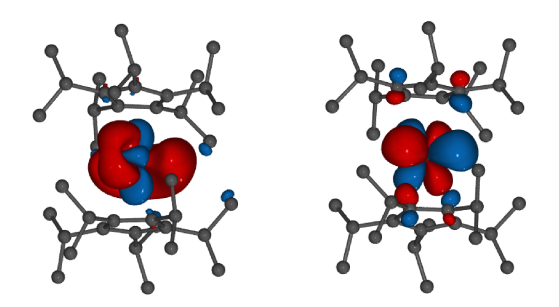


Figure 4: Contour plot of HOMO and LUMO for the divalent Pu metallocene at 0.03 isovalue computed with DFT. The predicted electron configuration is predominantly $(5f)^5$ with $6d_{z^2}$ and 7s admixture.

The Am, Bk, and No compounds adopt $(5f)^{n+1}$ ground states. This is due to the stabilization of the 5f orbitals with increasing nuclear charge, which is greater than ligand field stabilization of the 6d shell.⁵² The HOMO and LUMO contours for Bk are visualized in Figure 5, illustrating the assigned $(5f)^{n+1}$ configuration.

Table 2: Natural atomic populations of the HOMO arising from the An atom for $An(Cp^{iPr_5})_2$, (An = U, Pu, Bk).

	s	p	d	\mathbf{f}
U	0.388	0.000	0.408	0.000
Pu	$0.388 \\ 0.162$	0.017	0.168	0.538
Bk	0.000	0.000	0.000	0.959

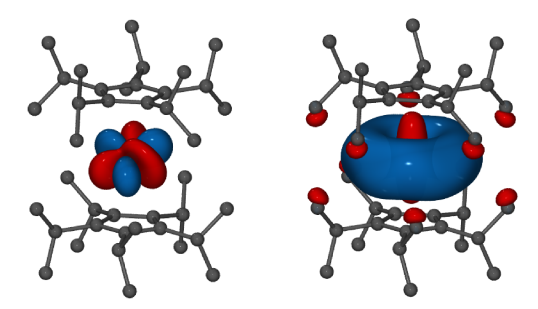


Figure 5: Contour plot of HOMO and LUMO for the Bk compound at 0.03 isovalue computed with DFT.

Molecular Structure and Bond Length

Highly symmetric structures with S_{10} symmetry were obtained for An = (Th, U, Bk, No, Lr). The S_{10} structures obtained for $Pu(Cp^{iPr_5})_2$ and $Am(Cp^{iPr_5})_2$ compounds are saddle points; subsequent optimization in C_1 symmetry resulted in slightly bent structures with dihedral angles of 11° and 12° as illustrated in Figure 6. Similar distortions were also observed in the crystal structure of $[Pu(Cp'')_3]^{-1}$, and may be rationalized as pseudo-Jahn-Teller effects indicating the presence of two nearly degenerate ground state configurations. The lower symmetry predicted for the Pu and Am compounds could be experimentally tested by structural and magnetic characterization.

The predicted metal-centroid bond lengths for $\operatorname{An}(\operatorname{Cp^{iPr_5}})_2$ are reported in Table 1. A decreasing trend across the actinide series is observed for compounds with both (6d) configurations (An = Th, U, Lr) and $(5f)^{n+1}$ configurations (An = Am, Bk, No), as expected due to f-block contraction. However, this trend is interrupted by the Pu and Am species showing an increase in metal-centroid distance compared to the earlier actinides. This may reflect the loss of bonding interactions with the ligand as the 6d orbital is depopulated and

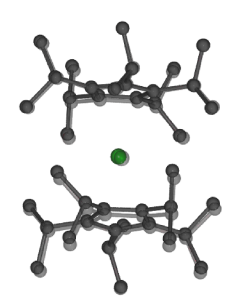


Figure 6: Converged structure of the Pu metallocene compound overlaid with the general S_{10} structure, computed with DFT. The structure deviates from linearity, leading to a dihedral angle of 11° .

an increased electron repulsion in the 5f shell.

In general, bond lengths were shorter than that observed for the corresponding tris-(Cp'/Cp'') compounds, $[An(Cp'/Cp'')_3]^{-1}$ (An = Th, U, Pu). These results are consistent with the lower coordination number of bis-coordinate compounds, and analogous to the decrease in bond lengths from tris(Cp') to $bis(Cp^{iPr_5})$ structures observed for the Ln(II) species. Compared to $U(COT)_2$ and $Th(COT)_2$, the $U(Cp^{iPr_5})_2$ and $Th(Cp^{iPr_5})_2$ metal-centroid distances are larger by 0.559 Å and 0.530 Å, respectively, which may be rationalized by the higher formal charge of the COT ligands compared to the present cyclopentadienyl ligands.

Absorption Spectra

Simulated electronic absorption spectra for $\operatorname{An}(\operatorname{Cp^{iPr_5}})_2$ (An = Th, U, Pu, Am, Bk, No, Lr) are reported in Figure 7. Detailed assignments are provided as SI. The spectra for $\operatorname{Th}(\operatorname{Cp^{iPr_5}})_2$ and $\operatorname{U}(\operatorname{Cp^{iPr_5}})_2$ show strong peaks in the UV-VIS region, which correspond to metal-ligand charge transfer (MLCT) excitations out of the $6d_{z^2}$ orbital transforming as a_g . Such excitations from a HOMO with 6d character are also observed for the $\operatorname{tris}(\operatorname{Cp'/Cp''})$ actinide and $\operatorname{bis}(\operatorname{Cp^{iPr_5}})$ lanthanide species.

Strong MLCT bands are not predicted for the spectra of Pu(Cp^{iPr₅})₂, Am(Cp^{iPr₅})₂,

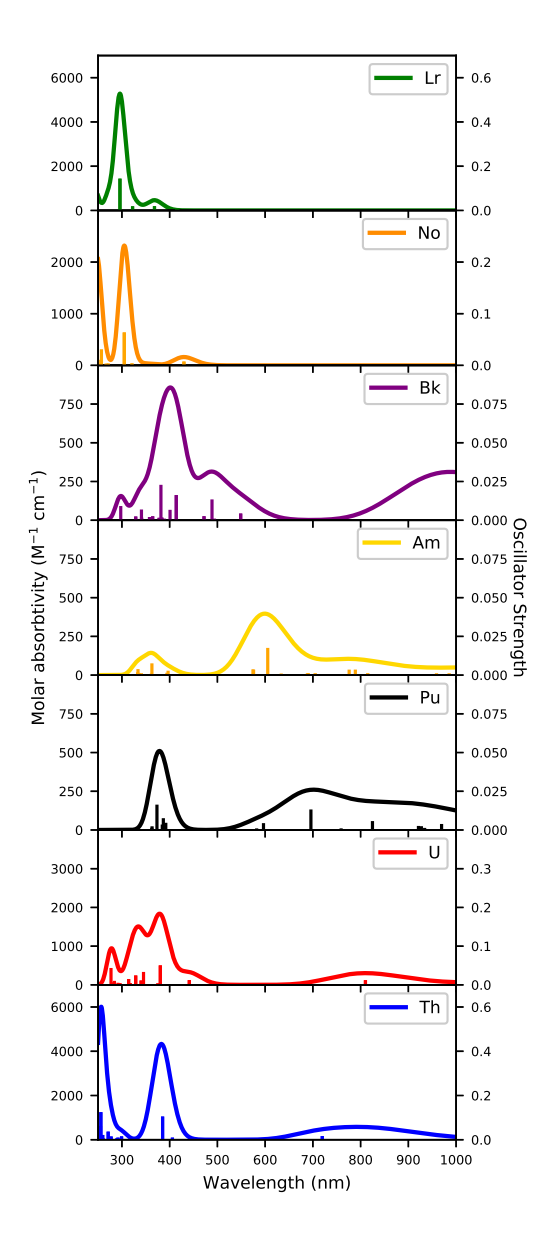


Figure 7: Comparison of absorption spectra for $An(Cp^{iPr_5})_2$ (An = Th, U, Pu, Am, Bk, No, Lr) computed with TD-DFT using the TPSSh functional. Spectra were fit using normalized Gaussians with a root mean square width of 0.15 and an empirical blue shift of 0.15 eV. These parameters are consistent with those used in the previous study of Ln(II) metallocenes. The broad peak in the infrared part of the spectrum for the Pu compound occurs off the plot at 1112 nm.

Bk(Cp^{iPr5})₂, and No(Cp^{iPr5})₂; instead, the main features are low intensity transitions from the occupied 5f shell to the 6d-type orbital transforming as e_{1g} . The Pu species exhibits small MLCT excitations out of the HOMO near 390 nm that are absent with the Am species, likely a consequence of its mixed orbital character. The f to d transition near 315 nm for No is more intense than that of other compounds with $(5f)^{n+1}$ configurations due to the closed shell ground state. Going across the series, $Lr(Cp^{iPr5})_2$ again exhibits strong MLCT excitations in the predicted spectral range, as expected from a $(6d)^1$ configuration.

For $An(Cp^{iPr_5})_2$ (An = Th, U, Pu, Am, Bk), a broad peak of low intensity in the 600 to 1000 nm region was observed. This peak was found to originate from a 6d to 5f transition for An = (Th, U) and a 5f to 6d transition for An = (Pu, Am, Bk). Such excitations are also present in the spectra of the Dy(II) and Tb(II) metallocenes. Peak maxima of common MLCT transitions between Th/U(Cp^{iPr_5})₂ and Dy/Tb(Cp^{iPr_5})₂ are slightly red-shifted, but otherwise remain in the same energy range.

Thermodynamic Stability

Synthetic feasibility of the bis(Cp^{iPr₅}) actinocenes can be assessed by considering their energetic stability, which is controlled by both kinetic and thermodynamic factors. Predicting kinetic stability, on the other hand, is much more difficult and typically requires knowledge of specific experimental conditions. Our discussion thus focuses mainly on thermodynamic stability of the bis(Cp^{iPr₅}) structures, which is a necessary but not a sufficient condition for their synthetic feasibility.

To investigate the thermodynamic stability of the bis(Cp^{iPr_5}) actinocenes, reduction of $[An(Cp^{iPr_5})_2]^+$ to obtain $An(Cp^{iPr_5})_2$ was modeled with DFT including solvation effects with COSMO. The trivalent bis(Cp^{iPr_5}) compound for uranium was isolated recently, ²⁰ indicating that these species may be stable synthetic precursors. For comparison, reduction of known $[Ln(Cp^{iPr_5})_2]^+$ (Ln = Tb, Dy) species was also studied. ^{35,53} Adiabatic reduction potentials including zero point energy and thermal corrections were computed from the free

energy differences of the metallocenium cations and corresponding neutral species. Optimized structures for the cations did not deviate significantly from those of the neutral species.

The absolute computed reduction potentials in Table 3 need to be interpreted with caution, since they refer to an artificial reference of a free electron in the gas phase, and may be affected strongly by errors inherent in the implicit solvation model used here. However, the results suggest that the reduction of cationic to neutral bis(Cp^{iPr₅}) actinide complexes is indeed thermodynamically favorable. Furthermore, these reduction potentials are of the same order as those computed for the analogous Tb and Dy compounds, suggesting that the actinocene complexes may be accessible by a similar synthetic route.

Table 3: Adiabatic reduction potentials for $An(Cp^{iPr_5})_2$ (An = Th, U, Pu, Am, Bk, No, Lr) and $Ln(Cp^{iPr_5})_2$ (Ln = Dy, Tb) computed with DFT using the TPSS functional and COSMO implicit solvation model.

	$E^{\circ}_{[An(Cp^{iPr_5})_2]^+-An(Cp^{iPr_5})_2}(eV)$
Th	2.78
U	3.99
Pu	4.20
Am	3.97
Bk	4.25
No	5.06
Lr	3.90
Dy	4.34
Tb	3.57

Monovalent Bis(Cyclopentadienyl) Actinides

To assess whether monovalent bis(cyclopentadienyl) actinide compounds might also be accessible, the adiabatic reduction potential of $Th(Cp^{iPr_5})_2$ was computed with the same methodology as the above. $Th(Cp^{iPr_5})_2$ was selected because it has an unoccupied 6d orbital with comparatively low orbital energy.

Optimized structures for the neutral and anionic species were obtained with DFT including COSMO solvent corrections. The additional electron of the anion was found to occupy

the metal-like 6d orbital transforming as e_{1g} . A slightly lower metal-centroid bond length of 2.52 Å was observed. Results are given in Table 4, and show that the 6d HOMO of the monovalent species remains bound. Furthermore, the calculated reduction potential suggests that anion formation is favored for this species.

To test if modification of the substituted cyclopentadienyl ligands with electron withdrawing groups could further stabilize this state, this energy calculation was repeated for optimized bis(pentafluorocyclopentadienyl) structures. A larger reduction potential is observed and the electron in the HOMO is further bound.

Table 4: Adiabatic reduction potentials and HOMO energy for $Th(Cp^{iPr_5})_2$ and $Th(C_5F_5)_2$ computed with DFT using the TPSS functional and COSMO implicit solvation model.

	$E^{\circ}(eV)$	$E_{\rm HOMO}({ m eV})$
$\operatorname{Th}(\operatorname{Cp}^{\mathrm{i}\operatorname{Pr}_5})_2$	1.93	-0.38
$Th(C_5F_5)_2$	2.30	-1.70

Conclusions

The present results suggest that the divalent actinocenes $\operatorname{An}(\operatorname{Cp^{iPr_5}})_2$ (An = Th, U, Pu, Am, Bk, No Lr) are worthwhile targets for synthesis and experimental characterization. If experimentally confirmed, these compounds would represent the first examples of low-valent cyclopentadienyl actinide complexes with linear or nearly linear coordination. In particular, the Th and U compounds appear promising for initial synthetic attempts, whereas synthetic access to the latter actinides is limited by their short lifetimes.

Both (5f) and (6d) ground state configurations were observed, with the Pu compound representing a borderline case. Further judicious ligand modifications could make it possible to extend the (6d) configuration to the later actinides, or even access the +1 oxidation state for the early actinides. The chemistry of these compounds is expected to be closer to that of transition metal metallocenes than typical actinide complexes in higher oxidation states. Potential applications include catalysis 54,55 and separation of nuclear fission products. 21,56

Given the unusual magnetic behavior of their lighter Dy and Tb congeners, ³⁵ actinocenes should also be evaluated for their suitability as single-molecule magnets.

Conflicts of Interest

Principal investigator Filipp Furche has an equity interest in Turbomole GmbH. The terms of this arrangement have been reviewed and approved by the University of California, Irvine, in accordance with its conflict of interest policies.

Acknowledgement

The authors would like to acknowledge William J. Evans and the group of Jeffrey R. Long for helpful comments and encouragement. This work was supported by NSF grant CHE-1800431. We thank the National Science Foundation Graduate Research Fellowship Program for support of J.M.Y.

Supporting Information Available

Molecular orbital contour plots, optimized geometry files, and electronic occupations can be found in the supporting information. A pre-print of this manuscript is available on Chemrxiv at (10.26434/chemrxiv.9640931.v1). This material is available free of charge via the Internet at http://pubs.acs.org/.

References

(1) Wilkinson, G.; Rosenblum, M.; Whiting, M.; Woodward, R. The structure of iron biscyclopentadienyl. J. Am. Chem. Soc. 1952, 74, 2125–2126.

- (2) Moffitt, W. The electronic structure of bis-cyclopentadienyl compounds. J. Am. Chem. Soc. 1954, 76, 3386–3392.
- (3) Kauffman, G. B. The discovery of ferrocene, the first sandwich compound. *J. Chem. Educ.* **1983**, *60*, 185.
- (4) Elschenbroich, C. Organometallics; John Wiley & Sons, 2016.
- (5) RajanBabu, T.; Nugent, W. A.; Taber, D. F.; Fagan, P. J. Stereoselective cyclization of enynes mediated by metallocene reagents. J. Am. Chem. Soc. 1988, 110, 7128–7135.
- (6) Kaminsky, W. The discovery of metallocene catalysts and their present state of the art. J. Polym. Sci., Part A: Polym. Chem. 2004, 42, 3911–3921.
- (7) Resconi, L.; Cavallo, L.; Fait, A.; Piemontesi, F. Selectivity in propene polymerization with metallocene catalysts. *Chem. Rev.* **2000**, *100*, 1253–1346.
- (8) Brintzinger, H. H.; Fischer, D.; Mülhaupt, R.; Rieger, B.; Waymouth, R. M. Stereospecific olefin polymerization with chiral metallocene catalysts. *Angew. Chem., Int. Ed. Engl.* **1995**, *34*, 1143–1170.
- (9) Chirik, P. J. Dinitrogen functionalization with bis (cyclopentadienyl) complexes of zirconium and hafnium. *Dalton Trans.* **2007**, 16–25.
- (10) Cotton, S. Lanthanide and actinide chemistry; John Wiley & Sons, 2013.
- (11) Neidig, M. L.; Clark, D. L.; Martin, R. L. Covalency in f-element complexes. *Coord. Chem. Rev.* **2013**, *257*, 394–406.
- (12) Fischer, R. D. Zur Metall-Ring-Bindung in Sandwich-Komplexen. *Theor. Chim. Acta* **1963**, *1*, 418–431.

- (13) Streitwieser, A.; Müller-Westerhoff, U.; Sonnichsen, G.; Mares, F.; Morrell, D.; Hodgson, K. O.; Harmon, C. Preparation and properties of uranocene, di-π-cyclooctatetraeneuranium(IV). J. Am. Chem. Soc. 1973, 95, 8644–8649.
- (14) Chang, A. H.; Pitzer, R. M. Electronic structure and spectra of uranocene. *J. Am. Chem. Soc.* **1989**, *111*, 2500–2507.
- (15) Seyferth, D. Uranocene. The first member of a new class of organometallic derivatives of the f elements. *Organometallics* **2004**, *23*, 3562–3583.
- (16) Moritz, A.; Dolg, M. Quasirelativistic 5f-in-core pseudopotential study of the actinocenes $An(C_8H_8)_2$, An = Th-Pu. Chem. Phys. **2007**, 337, 48–54.
- (17) Parry, J. S.; Cloke, F. G. N.; Coles, S. J.; Hursthouse, M. B. Synthesis and characterization of the first sandwich complex of trivalent thorium: A structural comparison with the uranium analogue. J. Am. Chem. Soc. 1999, 121, 6867–6871.
- (18) Maynadié, J.; Berthet, J.-C.; Thuéry, P.; Ephritikhine, M. An unprecedented type of linear metallocene with an f-element. J. Am. Chem. Soc. 2006, 128, 1082–1083.
- (19) Langeslay, R. R.; Windorff, C. J.; Dumas, M. T.; Ziller, J. W.; Evans, W. J. Thorium Metallocene cation chemistry: Synthesis and characterization of the bent $[(C_5Me_5)_2Th(C_6H_5)(THF)][BPh_4]$ and the parallel ring $[(C_5Me_5)_2Th(NCR)_5][BPh_4]_2$ (R= Me, Ph) complexes. Organometallics 2018, 37, 454–458.
- (20) Layfield, R.; Guo, F.-S.; Mansikkamaki, A.; Tong, M.-L.; Chen, Y.-C. Uranocenium: synthesis, structure and chemical bonding. *Angew. Chem.* **2019**,
- (21) Ephritikhine, M. Recent advances in organoactinide chemistry as exemplified by cyclopentadienyl compounds. *Organometallics* **2013**, *32*, 2464–2488.
- (22) Bursten, B. E.; Strittmatter, R. J. Cyclopentadienylactinide complexes: Bonding and electronic structure. *Angew. Chem., Int. Ed. Engl.* **1991**, *30*, 1069–1085.

- (23) Evans, W. J. Advances in f element reductive reactivity as a paradigm for expanding lanthanide and actinide science and technology. J. Alloys Compd. 2009, 488, 493–510.
- (24) Liddle, S. T. The renaissance of non-aqueous uranium chemistry. *Angew. Chem. Int. Ed.* **2015**, *54*, 8604–8641.
- (25) Evans, W. J. Tutorial on the role of cyclopentadienyl ligands in the discovery of molecular complexes of the rare-earth and actinide metals in new oxidation states.

 Organometallics 2016, 35, 3088–3100.
- (26) Hitchcock, P. B.; Lappert, M. F.; Maron, L.; Protchenko, A. V. Lanthanum does form stable molecular compounds in the +2 oxidation state. *Angew. Chem. Int. Ed.* **2008**, 47, 1488–1491.
- (27) MacDonald, M. R.; Bates, J. E.; Ziller, J. W.; Furche, F.; Evans, W. J. Completing the series of +2 ions for the lanthanide elements: synthesis of molecular complexes of Pr²⁺, Gd²⁺, Tb²⁺, and Lu²⁺. J. Am. Chem. Soc. **2013**, 135, 9857–9868.
- (28) Jenkins, T. F.; Woen, D. H.; Mohanam, L. N.; Ziller, J. W.; Furche, F.; Evans, W. J. Tetramethylcyclopentadienyl ligands allow isolation of Ln(II) ions across the lanthanide series in [K(2.2.2-cryptand)][(C₅Me₄H)₃Ln] complexes. *Organometallics* **2018**, *37*, 3863–3873.
- (29) Fieser, M. E.; MacDonald, M. R.; Krull, B. T.; Bates, J. E.; Ziller, J. W.; Furche, F.; Evans, W. J. Structural, spectroscopic, and theoretical comparison of traditional vs recently discovered Ln²⁺ ions in the [K(2.2.2 cryptand)][(C₅H₄SiMe₃)₃Ln] complexes: the variable nature of Dy²⁺ and Nd²⁺. J. Am. Chem. Soc. **2014**, 137, 369–382.
- (30) MacDonald, M. R.; Fieser, M. E.; Bates, J. E.; Ziller, J. W.; Furche, F.; Evans, W. J. Identification of the +2 oxidation state for uranium in a crystalline molecular complex, [K(2.2.2-cryptand)][(C₅H₄SiMe₃)₃U]. J. Am. Chem. Soc. **2013**, 135, 13310–13313.

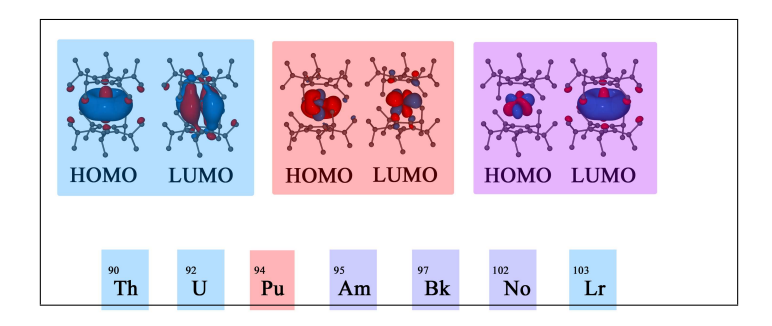
- (31) Windorff, C. J.; Chen, G. P.; Cross, J. N.; Evans, W. J.; Furche, F.; Gaunt, A. J.; Janicke, M. T.; Kozimor, S. A.; Scott, B. L. Identification of the formal +2 oxidation state of plutonium: synthesis and characterization of {Pu^{II}[C₅H₃(SiMe₃)₂]₃}⁻. J. Am. Chem. Soc. **2017**, 139, 3970–3973.
- (32) Langeslay, R. R.; Fieser, M. E.; Ziller, J. W.; Furche, F.; Evans, W. J. Synthesis, structure, and reactivity of crystalline molecular complexes of the {[C₅H₃(SiMe₃)₂]₃Th}

 ¹⁻ anion containing thorium in the formal +2 oxidation state. *Chem. Sci.* **2015**, *6*, 517–521.
- (33) Su, J.; Windorff, C. J.; Batista, E. R.; Evans, W. J.; Gaunt, A. J.; Janicke, M. T.; Kozimor, S. A.; Scott, B. L.; Woen, D. H.; Yang, P. Identification of the formal +2 oxidation state of neptunium: synthesis and structural characterization of $\{Np^{II}[C_5H_3(SiMe_3)_2]_3\}^{-1}$. J. Am. Chem. Soc. **2018**, 140, 7425–7428.
- (34) Evans, W. J.; Hughes, L. A.; Hanusa, T. P. Synthesis and crystallographic characterization of an unsolvated, monomeric bis(pentamethylcyclopentadienyl) organolanthanide complex,(C₅Me₅)₂Sm. J. Am. Chem. Soc. **1984**, 106, 4270–4272.
- (35) Gould, C.; McClain, R.; Yu, J.; Groshens, T.; Furche, F.; Harvey, B.; Long, J. Synthesis and magnetism of neutral, linear metallocene complexes of terbium(II) and dysprosium(II). J. Am. Chem. Soc. (accepted)
- (36) Ryan, A. J.; Darago, L. E.; Balasubramani, S. G.; Chen, G. P.; Ziller, J. W.; Furche, F.; Long, J. R.; Evans, W. J. Synthesis, structure, and magnetism of tris(amide)[Ln{N(SiMe₃)₂}₃]¹⁻ complexes of the non-traditional +2 lanthanide ions. *Chem.: Eur. J.* **2018**, 24, 7702–7709.
- (37) Siladke, N. A.; Meihaus, K. R.; Ziller, J. W.; Fang, M.; Furche, F.; Long, J. R.; Evans, W. J. Synthesis, structure, and magnetism of an f element nitrosyl complex, (C₅Me₄H)₃UNO. J. Am. Chem. Soc. 2011, 134, 1243–1249.

- (38) Tao, J.; Perdew, J. P.; Staroverov, V. N.; Scuseria, G. E. Climbing the density functional ladder: Nonempirical meta-generalized gradient approximation designed for molecules and solids. *Phys. Rev. Lett.* **2003**, *91*, 146401.
- (39) Dolg, M.; Cao, X. Accurate relativistic small-core pseudopotentials for actinides. Energy adjustment for uranium and first applications to uranium hydride. *J. Phys. Chem. A* **2009**, *113*, 12573–12581.
- (40) Cao, X.; Dolg, M.; Stoll, H. Valence basis sets for relativistic energy-consistent small-core actinide pseudopotentials. *J. Chem. Phys.* **2003**, *118*, 487–496.
- (41) Cao, X.; Dolg, M. Segmented contraction scheme for small-core actinide pseudopotential basis sets. *J. Mol. Struct.: THEOCHEM* **2004**, *673*, 203–209.
- (42) Weigend, F.; Ahlrichs, R. Balanced basis sets of split valence, triple zeta valence and quadruple zeta valence quality for H to Rn: Design and assessment of accuracy. *Phys. Chem. Chem. Phys.* 2005, 7, 3297–3305.
- (43) Weigend, F.; Köhn, A.; Hättig, C. Efficient use of the correlation consistent basis sets in resolution of the identity MP2 calculations. *J. Chem. Phys.* **2002**, *116*, 3175–3183.
- (44) Grimme, S.; Antony, J.; Ehrlich, S.; Krieg, H. A consistent and accurate ab initio parametrization of density functional dispersion correction (DFT-D) for the 94 elements H-Pu. J. Chem. Phys. 2010, 132, 154104.
- (45) Deglmann, P.; Furche, F.; Ahlrichs, R. An efficient implementation of second analytical derivatives for density functional methods. *Chem. Phys. Lett.* **2002**, *362*, 511–518.
- (46) Reed, A. E.; Weinstock, R. B.; Weinhold, F. Natural population analysis. *J. Chem. Phys.* **1985**, *83*, 735–746.
- (47) Bates, J. E.; Furche, F. Harnessing the meta-generalized gradient approximation for time-dependent density functional theory. *J. Chem. Phys.* **2012**, *137*, 164105.

- (48) Klamt, A.; Schüürmann, G. COSMO: a new approach to dielectric screening in solvents with explicit expressions for the screening energy and its gradient. *J. Am. Chem. Soc.* **1993**, 799–805.
- (49) Lide, D. R. CRC handbook of chemistry and physics, 81st ed.; CRC press: Boca Raton, 2008; p 136.
- (50) Humphrey, W.; Dalke, A.; Schulten, K. VMD Visual Molecular Dynamics. J. Mol. Graph. 1996, 14, 33–38.
- (51) Furche, F.; Ahlrichs, R.; Hättig, C.; Klopper, W.; Sierka, M.; Weigend, F. Turbomole. Wiley Interdiscip. Rev. Comput. Mol. 2014, 4, 91–100.
- (52) Fricke, B.; Greiner, W.; Waber, J. The continuation of the periodic table up to Z=172. The chemistry of superheavy elements. *Theor. Chim. Acta* 1971, 21, 235–260.
- (53) McClain, K. R.; Gould, C. A.; Chakarawet, K.; Teat, S. J.; Groshens, T. J.; Long, J. R.; Harvey, B. G. High-temperature magnetic blocking and magneto-structural correlations in a series of dysprosium(III) metallocenium single-molecule magnets. *Chem. Sci.* 2018, 9, 8492–8503.
- (54) Fox, A. R.; Bart, S. C.; Meyer, K.; Cummins, C. C. Towards uranium catalysts. *Nature* **2008**, *455*, 341.
- (55) Arnold, P. L.; Turner, Z. R. Carbon oxygenate transformations by actinide compounds and catalysts. *Nature Rev. Chem.* **2017**, *1*, 0002.
- (56) Kaltsoyannis, N. Does covalency increase or decrease across the actinide series? Implications for minor actinide partitioning. *Inorg. Chem.* **2012**, *52*, 3407–3413.

Graphical TOC Entry



1 TOC synopsis

Density functional theory calculations suggest that linear bis(pentaisopropylcyclopentadienyl) actinocenes are worthwhile synthetic targets.